Higgs dynamics in the early universe

Vis, J.M. van de

Chapter 4

Preheating after Higgs inflation: self-resonance and gauge boson production

4.1 Introduction

In this chapter we study the production of Standard Model particles after inflation caused by the Higgs field. The intriguing possibility of identifying the Higgs field with the scalar field driving inflation requires a non-minimal coupling between the Higgs field and the Ricci curvature scalar $\mathcal{L} \supset \frac{1}{2}R(m_{\rm pl}^2 + 2\xi\Phi^\dagger\Phi)$ [155]. We are already familiar with this coupling from chapter 3, but note that the non-minimal-coupling term needed for Higgs inflation has a different sign than the term used in chapter 3 (see eq. (3.4)). In both chapters we study positive values of ξ.

Since Higgs inflation is not feasible for negative values of the Higgs self-coupling λ, in this chapter we will assume that it is positive. The measured value of the amplitude of scalar perturbations determines the value of λ/ξ^2. The inherent ambiguity in the running of λ at high energies, due to our incomplete knowledge of possible new physics between the TeV and inflationary scales, leads to an ambiguity in the exact value of the required non-minimal coupling [156–160]. While simple estimates like $\lambda_{\rm infl} = \mathcal{O}(0.01)$ lead to the requirement of $\xi = \mathcal{O}\left(10^4\right)$, smaller values of λ can allow for much smaller non-minimal couplings. We will remain agnostic about the exact running of the Standard Model couplings at high energies and instead explore a broad parameter range[1]

[1]For inflation on the flat plateau one should consider $\xi \gtrsim 440$ (e.g. [161]). In models of hilltop or inflection point inflation, smaller values of ξ are possible, although UV corrections are expected to be larger. A discussion of the effects of UV corrections, as well as initial conditions, in Higgs inflation can be found for example in Refs. [162, 163]. In order to provide a treatment of Higgs inflation as complete as possible without referring to specific unknown physics, we choose to consider a broad range of non-minimal couplings that go below $\xi \approx 400$.

covering $10 \lesssim \xi \lesssim 10^4$.

A basic feature of inflationary models with non-minimal couplings is that they provide universal predictions for the spectral observables n_s and r, largely independent of the exact model parameters and initial conditions [164, 165]. These observables fall in line with the Starobinsky model [136] as well as with the large family of α-attractors [166–170]. Even after the latest Planck release [77], these models, which predict $n_s = 1 - 2/N_*$ and $r = \mathcal{O}(1/N_*^2)$, continue to be compatible with the data for modes that exit the horizon at $N_* \simeq 55$ e-folds before the end of inflation.

Higgs inflation provides a unique opportunity to study the transition from inflation to radiation domination, since the couplings of the Higgs-inflaton to the rest of the SM are known. Detailed analyses of reheating in Higgs inflation were first performed in Refs. [171, 172] and extended in Ref. [173] using lattice simulations. However, as discussed later in Refs. [174–176] and independently in Ref. [177], multi-field models of inflation with non-minimal couplings to gravity can exhibit more efficient preheating behavior than previously thought, due to the contribution of the field-space structure to the effective mass of the fluctuations. Furthermore, it was shown in Refs. [174–176] that, in non-minimally coupled models, preheating efficiency can be vastly different for different values of the non-minimal coupling, even if these values lead to otherwise identical predictions for CMB observables. We will thus perform a detailed study of preheating in Higgs inflation, extending the results of Refs. [171, 172, 174–177], in order to distinguish between Higgs inflation models with different values of the non-minimal coupling.

Because of the appeal of Higgs inflation as an economical model of realizing inflation within the particle content of the Standard Model, the unitarity cutoff scale of the theory has been extensively studied [159, 160, 178–190] (see also Ref. [191] for a recent review). For large values of the Higgs vev, like the ones appearing during inflation on the flat plateau, the appropriate unitarity cutoff scale is $m_{\rm pl}/\sqrt{\xi}$, while for small values of the Higgs vev it must be substituted by $m_{\rm pl}/\xi$.

In section 4.2, we introduce a simplified model of a complex Higgs field coupled to an Abelian gauge field. We also discuss the relation to the full SM gauge sector. In section 4.3 we study self-resonance of Higgs modes. Section 4.4 deals with the evolution of the gauge fields during and after Higgs inflation. At the end of this section we also address the unitarity scale. The effect of decays and scattering processes that involve the produced Higgs and gauge bosons are summarized in section 4.5 and observational consequences in 4.6. Concluding remarks follow in section 4.7. This chapter is a modified version of our work [2]. We will occasionally omit some details and refer to the original paper.

4.2 Abelian model and formalism

We build on the formalism of Ref. [192] for the evolution of non-minimally coupled multi-field models, as it was applied in Refs. [164, 193, 194] during inflation and in Refs. [174–176] during preheating. The electroweak sector consists of a complex Higgs doublet, expressed using 4 real-valued scalar fields in $3+1$ spacetime dimensions:

$$\Phi = \frac{1}{\sqrt{2}} \begin{pmatrix} \theta^1 + i\theta^2 \\ \varphi + h + i\theta \end{pmatrix} , \tag{4.1}$$

where φ is the background value of the Higgs field, h denotes the Higgs fluctuations and θ, θ^1 and θ^2 are the Goldstone modes. In order to study decay into gauge bosons, we add the $SU(2)_L$ and $U(1)_Y$ gauge sectors. We will start by closely examining a simplified Abelian model as a proxy for the full electroweak sector, consisting of the complex scalar field

$$\Phi = \frac{1}{\sqrt{2}}(\varphi + h + i\theta), \tag{4.2}$$

and a $U(1)$ gauge field only. We discuss the relation between this simplified Abelian model and the equations of the full Higgsed electroweak sector in section 4.2.3.

In order to connect our notation to that of Ref. [192] we identify $\phi^1 = \varphi + h$ and $\phi^2 = \theta$. We will start by deriving the equations of motion for general ϕ^I-fields for notational simplicity. We use upper-case Latin letters to label field-space indices, $I, J = 1, 2, 3, 4$ (or just $I, J = 1, 2$ in the Abelian case); Greek letters to label spacetime indices, $\mu, \nu = 0, 1, 2, 3$; and lower-case Latin letters to label spatial indices, $i, j = 1, 2, 3$.

We first consider $U(1)$ symmetry with the corresponding gauge field B_μ. The Lagrangian in the Jordan frame is given by

$$S_J = \int d^4x\sqrt{-\tilde{g}}\Big[f(\Phi,\Phi^\dagger)\tilde{R} - \tilde{g}^{\mu\nu}(\tilde{\nabla}_\mu\Phi)^\dagger\tilde{\nabla}_\nu\Phi - \frac{1}{4}\tilde{g}^{\mu\rho}\tilde{g}^{\nu\sigma}F_{\mu\nu}F_{\rho\sigma} - \tilde{V}(\Phi,\Phi^\dagger)\Big] . \tag{4.3}$$

The covariant derivative $\tilde{\nabla}_\mu$ is given by

$$\tilde{\nabla}_\mu = \tilde{D}_\mu + ieB_\mu, \tag{4.4}$$

where $\tilde{D}_\mu$ is a covariant derivative with respect to the space-time metric $\tilde{g}_{\mu\nu}$ and e is the coupling constant. The corresponding field strength tensor[2] is

$$F_{\mu\nu} = \tilde{D}_\mu B_\nu - \tilde{D}_\nu B_\mu. \tag{4.5}$$

By performing a conformal transformation

$$\tilde{g}_{\mu\nu}(x) \to g_{\mu\nu}(x) = \frac{2}{m_{\rm pl}^2} f(\Phi, \Phi^\dagger)\, \tilde{g}_{\mu\nu}(x), \tag{4.6}$$

the action in the Einstein frame becomes

$$\begin{aligned} S = \int d^4x\sqrt{-g}\Bigg[& \frac{m_{\rm pl}^2}{2} R - g^{\mu\nu}\Big(\frac{1}{2}\mathcal{G}_{IJ}(\Phi,\Phi^\dagger) D_\mu\phi^I D_\nu\phi^J + \frac{m_{\rm pl}^2}{2f(\Phi,\Phi^\dagger)} \\ & \Big((ieB_\mu\Phi)^\dagger (ieB_\nu\Phi) + ie(-B_\mu\Phi^\dagger D_\nu\Phi + B_\nu(D_\mu\Phi^\dagger)\Phi)\Big)\Big) - V(\Phi,\Phi^\dagger) - \frac{1}{4} g^{\mu\rho} g^{\nu\sigma} F_{\mu\nu} F_{\rho\sigma}\Bigg], \end{aligned} \tag{4.7}$$

with

$$V(\Phi,\Phi^\dagger) = \frac{m_{\rm pl}^4}{4f^2(\Phi,\Phi^\dagger)} \tilde{V}(\Phi,\Phi^\dagger), \tag{4.8}$$

and

$$\mathcal{G}_{IJ}(\Phi,\Phi^\dagger) = \frac{m_{\rm pl}^2}{2f(\Phi,\Phi^\dagger)} \left[\delta_{IJ} + \frac{3}{f(\Phi,\Phi^\dagger)} f(\Phi,\Phi^\dagger)_{,I}\, f(\Phi,\Phi^\dagger)_{,J}\right], \tag{4.9}$$

as in Refs. [192, 193]. The subscript $,I$ denotes a derivative with respect to the field ϕ^I. The potential in the Jordan frame is the usual Standard Model Higgs potential

$$\tilde{V}(\Phi,\Phi^\dagger) = \lambda\left(\Phi^\dagger\Phi - \frac{1}{2}v_0^2\right)^2 \simeq \lambda\left(\Phi^\dagger\Phi\right)^2, \tag{4.10}$$

where the Higgs vacuum expectation value $v_0 = 246\,\text{GeV}$ can be safely neglected at field values that arise during inflation and preheating. Hence the Higgs potential can be adequately modeled by a pure quartic term.

[2]The tensor $F_{\mu\nu}$ is defined with lower indices. In that case it does not matter whether partial or covariant derivatives are used. However, when working with $\tilde{F}^{\mu\nu}$ it *does* matter, since the metric does not commute with partial derivatives. So $\tilde{F}^{\mu\nu}$ is given by $\tilde{F}^{\mu\nu} = \tilde{g}^{\mu\rho}\tilde{g}^{\nu\sigma}F_{\rho\sigma} = \tilde{g}^{\mu\rho}\tilde{g}^{\nu\sigma}(\tilde{D}_\rho B_\sigma - \tilde{D}_\sigma B_\rho) = \tilde{D}^\mu B^\nu - \tilde{D}^\nu B^\mu$.

For the sake of readability, we will drop the arguments of $\mathcal{G}, V$ and f from now on. Varying the action with respect to the scalar fields ϕ^I, the corresponding equation of motion for ϕ^I is

$$\begin{aligned}\Box\phi^I + g^{\mu\nu}\Gamma^I_{JK}\partial_\mu\phi^J\partial_\nu\phi^K + \mathcal{G}^{IJ}\left(\left(\frac{m_{\rm pl}^4}{4\xi f}e^2B^2\right)_{,J} - V_{,J}\right) + ie\frac{m_{\rm pl}^2}{2f^2}f_{,J}\,\mathcal{G}^{IJ}\Big(- B^\mu\Phi^\dagger D_\mu\Phi \\ + B^\mu(D_\mu\Phi^\dagger)\Phi\Big) - iem_{\rm pl}^2\mathcal{G}^{IJ}\Bigg(- \frac{1}{2f}B^\mu\Phi^\dagger{}_{,J}\,D_\mu\Phi + D_\mu\left(\frac{1}{2f}B^\mu\Phi^\dagger\right)\Phi_{,J} \\ - \Phi^\dagger{}_{,J}\,D_\mu\left(\frac{1}{2f}B^\mu\Phi\right) + \frac{1}{2f}B^\mu\left(D_\mu\Phi^\dagger\right)\Phi_{,J}\Bigg) = 0.\end{aligned} \tag{4.11}$$

We work to first order in fluctuations, in both the scalar fields and spacetime metric. The gauge fields have no background component, thus we only treat them as first-order perturbations. We consider scalar metric perturbations around a spatially flat FLRW metric,

$$\begin{aligned}ds^2 &= g_{\mu\nu}(x)\,dx^\mu dx^\nu \\ &= -(1+2A)dt^2 + 2a\,(\partial_i\mathcal{B})\,dx^i dt + a^2\left[(1-2\psi)\delta_{ij} + 2\partial_i\partial_j E\right]dx^i dx^j,\end{aligned} \tag{4.12}$$

where $a(t)$ is the scale factor. We may always choose a coordinate transformation and eliminate two of the four scalar metric functions that appear in eq. (4.12). We work in the longitudinal gauge, where $\mathcal{B}(x) = E(x) = 0$. Furthermore, in the absence of anisotropic pressure perturbations, the remaining two functions are equal $A(x) = \psi(x)$.

We also expand the fields,

$$\phi^I(x^\mu) = \varphi^I(t) + \delta\phi^I(x^\mu). \tag{4.13}$$

Note that for Higgs inflation only ϕ^1 has a background value, $\varphi(t)$, whereas the background value of ϕ^2 is zero.

We may then construct generalizations of the Mukhanov-Sasaki variable that are invariant with respect to spacetime gauge transformations up to first order in the perturbations [192, 195–197]:

$$Q^I = \delta\phi^I + \frac{\dot\varphi^I}{H}\psi. \tag{4.14}$$

The background equation of motion for φ^I is unchanged with respect to models with multiple scalar fields and no gauge bosons

$$\mathcal{D}_t\dot\varphi^I + 3H\dot\varphi^I + \mathcal{G}^{IJ}V_{,J} = 0\,, \tag{4.15}$$

and

$$\begin{aligned} H^2 &= \frac{1}{3m_{\rm pl}^2}\left[\frac{1}{2}\mathcal{G}_{IJ}\dot{\varphi}^I\dot{\varphi}^J + V(\varphi^I)\right], \\ \dot{H} &= -\frac{1}{2m_{\rm pl}^2}\mathcal{G}_{IJ}\dot{\varphi}^I\dot{\varphi}^J, \end{aligned} \tag{4.16}$$

where overdots denote derivatives with respect to t, and the Hubble parameter is given by $H(t) = \dot{a}/a$. Covariant derivatives with respect to the field-space metric are given by $\mathcal{D}_J A^I = \partial_J A^I + \Gamma^I_{\ JK} A^K$ for a field-space vector[3] A^I, from which we may construct the (covariant) directional derivative with respect to cosmic time,

$$\mathcal{D}_t A^I = \dot{\varphi}^J \mathcal{D}_J A^I = \dot{A}^I + \Gamma^I_{\ JK}\dot{\varphi}^J A^K\,, \tag{4.17}$$

where the Christoffel symbols $\Gamma^I_{\ JK}(\varphi^L)$ are constructed from $\mathcal{G}_{IJ}(\varphi^K)$.

We now specify our analysis to the case of a complex Higgs field with background $\varphi(t)$ and fluctuations $h(t,\vec{x})$ and $\theta(t,\vec{x})$ as in eq. (4.2). The equation of motion for the gauge-invariant fluctuation Q^I is identical to the case without the presence of a gauge-field [174–176, 192], up to terms that mix θ and B_μ:

$$\begin{aligned} &\mathcal{D}_t^2 Q^I + 3H\mathcal{D}_t Q^I + \left[\frac{k^2}{a^2}\delta^I_J + \mathcal{M}^I{}_J\right] Q^J \\ &- e\frac{m_{\rm pl}^2}{2f}\mathcal{G}^{IJ}\frac{d\theta}{d\phi^J}\left(2B^\mu\partial_\mu\varphi + (D_\mu B^\mu)\varphi + 2fB^\mu\varphi D_\mu\left(\frac{1}{2f}\right)\right) = 0, \end{aligned} \tag{4.18}$$

where we define the mass-squared matrix by

$$\mathcal{M}^I_{\ J} \equiv \mathcal{G}^{IK}\left(\mathcal{D}_J\mathcal{D}_K V\right) - \mathcal{R}^I_{\ LMJ}\dot{\varphi}^L\dot{\varphi}^M - \frac{1}{m_{\rm pl}^2 a^3}\mathcal{D}_t\left(\frac{a^3}{H}\dot{\varphi}^I\dot{\varphi}_J\right), \tag{4.19}$$

and $\mathcal{R}^I_{\ LMJ}$ is the Riemann tensor constructed from the field-space metric $\mathcal{G}_{IJ}(\varphi^K)$. The term in eq. (4.19) proportional to $1/m_{\rm pl}^2$ arises from the coupled metric perturbations through expanding Einstein's field equations to linear order and using eq. (4.14). It hence vanishes in the limit of an infinitely rigid spacetime $m_{\rm pl} \to \infty$. In the single field attractor [164, 174, 193], the background field motion proceeds along a straight single-field trajectory $\varphi(t)$. $\mathcal{G}^{IJ}$ and $\mathcal{M}^{IJ}$ are then diagonal

[3] Examples of field-space vectors include $A^I = \delta\phi^I$ and $A^I = \dot{\varphi}^I$.

at background order, so the equations of motion for the first order fluctuations h and θ do not mix:

$$\begin{aligned}
&\mathcal{D}_t^2 Q^h + 3H\mathcal{D}_t Q^h + \left[\frac{k^2}{a^2} + \mathcal{M}^h{}_h\right] Q^h = 0, \\
&\mathcal{D}_t^2 Q^\theta + 3H\mathcal{D}_t Q^\theta + \left[\frac{k^2}{a^2} + \mathcal{M}^\theta{}_\theta\right] Q^\theta \\
&- e\frac{m_{\rm pl}^2}{2f}\mathcal{G}^{\theta\theta}\left(2B^\mu\partial_\mu\varphi + (D_\mu B^\mu)\varphi + 2fB^\mu\varphi D_\mu\left(\frac{1}{2f}\right)\right) = 0,
\end{aligned} \tag{4.20}$$

where

$$Q^h = h + \frac{\dot\varphi}{H}\Psi, \qquad Q^\theta = \theta. \tag{4.21}$$

We see that only the Higgs fluctuations, generated along the direction of background motion, are coupled to the metric perturbations Ψ. In the language of Refs. [174–176], the Higgs fluctuations correspond to adiabatic modes.

The equations are simplified if we replace $Q^I \to X^I/a(t)$ and use covariant derivatives with respect to conformal time τ instead of cosmic time. We multiply the equations by a^3 and obtain:

$$\mathcal{D}_\tau^2 X^h + (k^2 + a^2(\mathcal{M}^h{}_h - \frac{1}{6}R\mathcal{G}^h{}_h))X^h = 0, \tag{4.22}$$

$$\mathcal{D}_\tau^2 X^\theta + (k^2 + a^2(\mathcal{M}^\theta{}_\theta - \frac{1}{6}R\mathcal{G}^\theta{}_\theta))X^\theta - ea^3\frac{m_{\rm pl}^2}{2f}\mathcal{G}^{\theta\theta}(2B^0\dot\varphi + (D_\mu B^\mu)\varphi - \frac{\dot f}{f}B^0\varphi) = 0\,. \tag{4.23}$$

Variation of the action with respect to the gauge field gives

$$D_\nu F^{\nu\mu} - \frac{m_{\rm pl}^2 e^2}{f}\Phi^\dagger\Phi B^\mu + ie\frac{m_{\rm pl}^2}{2f}g^{\mu\nu}(\Phi^\dagger\partial_\nu\Phi - (\partial_\nu\Phi^\dagger)\Phi) = 0. \tag{4.24}$$

Since there is no background value for the gauge field, the first order perturbation equation is:

$$D_\nu F^{\nu\mu} - \frac{m_{\rm pl}^2 e^2}{2f}\varphi^2 B^\mu + e\frac{m_{\rm pl}^2}{2f}g^{\mu\nu}(\theta\partial_\nu\varphi - \varphi\partial_\nu\theta) = 0, \tag{4.25}$$

where we used eq. (4.2) and we stress again that $F^{\nu\mu}$ is defined using covariant derivatives.

Until now we have worked in full generality, not choosing a gauge. Hence we are in principle working with more degrees of freedom than needed. We will distinguish two frequently used gauges: unitary and Coulomb gauge. The equation of motion of X^h is unaffected by the gauge choice.

4.2.1 Unitary gauge

In unitary gauge $\theta = 0 = X^\theta$. We go to Fourier space, with convention $f(x) = \int \frac{d^3\mathbf{k}}{(2\pi)^{3/2}} f_\mathbf{k} e^{-i\mathbf{k}\cdot\mathbf{x}}$ and split the field into a transverse ($B_k^\pm$) and longitudinal (B_k^L) mode:

$$\vec{B}_\mathbf{k} = \hat{\epsilon}^L_\mathbf{k} B^L_\mathbf{k} + \hat{\epsilon}^+_\mathbf{k} B^+_\mathbf{k} + \hat{\epsilon}^-_\mathbf{k} B^-_\mathbf{k} \,, \tag{4.26}$$

with

$$i\mathbf{k}\cdot\hat{\epsilon}^L_\mathbf{k} = |\mathbf{k}|, \qquad \mathbf{k}\cdot\hat{\epsilon}^\pm_\mathbf{k} = 0 \,. \tag{4.27}$$

The equations of motion for the transverse and longitudinal modes become (see Ref. [2] for a derivation):

$$\begin{aligned} &\partial_\tau^2 B^\pm_\mathbf{k} + (k^2 + a^2 \frac{m_{\rm pl}^2 e^2}{2f}\varphi^2) B^\pm_\mathbf{k} = 0 \,, \\ &\partial_\tau^2 B^L_\mathbf{k} + 2\left(\frac{\partial_\tau\varphi}{\varphi} - \frac{\partial_\tau f}{2f} + \frac{\partial_\tau a}{a}\right) \frac{k^2}{k^2 + \frac{m_{\rm pl}^2 a^2}{2f} e^2\varphi^2} \partial_\tau B^L_\mathbf{k} + (k^2 + a^2 \frac{m_{\rm pl}^2 e^2}{2f}\varphi^2) B^L_\mathbf{k} = 0 \,. \end{aligned} \tag{4.28}$$

4.2.2 Coulomb gauge

In Coulomb gauge ($\partial_i B^i = 0$), the Goldstone mode θ remains an explicit dynamical degree of freedom and the equation of motion for X^θ is:

$$\begin{aligned} &\mathcal{D}_\tau^2 X^\theta - 2e^2 \frac{m_{\rm pl}^4}{4f^2} \mathcal{G}^{\theta\theta} \frac{\varphi(\partial_\tau\varphi - \frac{\partial_\tau f}{2f}\varphi + \frac{\partial_\tau a}{a}\varphi)}{\frac{k^2}{a^2} + \frac{m_{\rm pl}^2 e^2\varphi^2}{2f}} \mathcal{D}_\tau X^\theta \\ &+ \left(k^2 + a^2(\mathcal{M}^\theta{}_\theta - \frac{1}{6} R \mathcal{G}^\theta{}_\theta) + e^2 \frac{m_{\rm pl}^4}{4f^2} \mathcal{G}^{\theta\theta} \Big(a^2\varphi^2 + 2 \frac{(\partial_\tau\varphi - \frac{\partial_\tau f}{2f}\varphi + \frac{\partial_\tau a}{a}\varphi)(\partial_\tau\varphi + \frac{\partial_\tau a}{a}\varphi)}{\frac{k^2}{a^2} + \frac{m_{\rm pl}^2 e^2}{2f}\varphi^2} \right. \\ &\left. + 2 \frac{\partial_\tau\varphi\varphi(\partial_\tau\varphi - \frac{\partial_\tau f}{2f}\varphi + \frac{\partial_\tau a}{a}\varphi)}{\frac{k^2}{a^2} + \frac{m_{\rm pl}^2 e^2}{2f}\varphi^2} \Gamma^\theta_{h\theta} \Big) \right) X^\theta = 0 \,. \end{aligned} \tag{4.29}$$

We must demand that physical observables are identical in the two gauges, and derive a relation between $\theta_\mathbf{k}$ in Coulomb gauge and $B^L_\mathbf{k}$ in unitary gauge. $X^h_\mathbf{k}$ and $B^\pm_\mathbf{k}$ are already identical in the two gauges. The longitudinal component of the electric field[4] is given by

$$E^L_\mathbf{k} = \dot{B}^L_\mathbf{k} - k B_{0,\mathbf{k}}. \tag{4.30}$$

[4]The gauge field being studied is not the $U(1)_Q$ of the electromagnetic sector. However, we will use the familiar nomenclature found in electromagnetism.

In unitary and Coulomb gauge we get

$$\text{Unitary:} \quad E^L_{\mathbf{k}} = \frac{m_{\rm pl}^2 e^2}{2f}\varphi^2 \frac{\dot{B}^L_{\mathbf{k}}}{\frac{k^2}{a^2} + \frac{m_{\rm pl}^2 e^2}{2f}\varphi^2}, \qquad \text{Coulomb:} \quad E^L_{\mathbf{k}} = -k\frac{m_{\rm pl}^2 e}{2f} \frac{\theta_{\mathbf{k}}\dot{\varphi} - \varphi\dot{\theta}_{\mathbf{k}}}{\frac{k^2}{a^2} + \frac{m_{\rm pl}^2 e^2}{2f}\varphi^2}. \tag{4.31}$$

Since E_L should not depend on the gauge, we can use these expressions to solve for B_L in terms of θ. We obtain

$$B^L_{\mathbf{k}} = \frac{k}{e\varphi}\theta_{\mathbf{k}}. \tag{4.32}$$

It is interesting to note that there is no ξ-dependent term in the relation of $\theta_{\mathbf{k}}$ to $B^L_{\mathbf{k}}$. It is a straightforward algebraic exercise to show that by using eq. (4.32), the equation of motion for $B^L_{\mathbf{k}}$ and $\theta_{\mathbf{k}}$ can be transformed into each other, providing a useful check for our derivation.

During preheating, when the background inflaton field oscillates, the unitary gauge becomes ill-defined at the times where $\varphi(t) = 0$, as can be seen for example in the transformation relation of eq. (4.32). We will perform preheating simulations is the Coulomb gauge, which is always well-defined.

4.2.3 Full $SU(2)_L \times U(1)_Y$-sector

In section 3 of Ref. [2] we compute the equations of motion for the full Higgsed electroweak sector. To first order in fluctuations non-Abelian effects are absent and the equations of motion derived above can easily be translated to the full electroweak case. The equations of motion of the background field φ and the Higgs boson h do not change. The photon does not couple to the Higgs field and its equation of motion $D_\nu F^{\nu\mu} = 0$ is therefore unaffected.

In unitary gauge the relevant degrees of freedom are the transverse and longitudinal polarizations of the W- and Z-bosons. Their equations of motion are identical to eqs. (4.28) with the replacement $e^2 \to \frac{g^2}{2}$ for the W and $e^2 \to \frac{g^2}{4\cos^2\theta_W}$ for the Z, where g is the $SU(2)$ coupling constant and θ_W the Weinberg angle.

In Coulomb gauge the equations of motion for the transverse polarizations of W and Z are the same as in unitary gauge. The equation of motion of the Goldstone mode θ is obtained from eq. (4.29) by the replacement $e^2 \to \frac{g^2}{4\cos^2\theta_W}$. The equations for the other Goldstone modes $\phi^I = \theta^1, \theta^2$ are obtained from eq. (4.29) by replacing $e^2 \to \frac{g^2}{4}$ and the field-space-dependent quantities $\mathcal{G}^{\theta\theta} \to \mathcal{G}^{\phi^I\phi^I}$ and $\Gamma^\theta_{h\theta} \to \Gamma^{\phi^I}_{h\phi^I}$.

For simplicity, we will work with the Abelian equations derived in section 4.2 in the rest of this chapter.

4.2.4 Single-field attractor and parameter choices

For Higgs inflation, the function $f(\Phi, \Phi^\dagger)$ is given by [155]:

$$f(\Phi, \Phi^\dagger) = \frac{m_{\rm pl}^2}{2} + \xi \Phi^\dagger \Phi. \tag{4.33}$$

For typical values of Higgs inflation $\lambda = \mathcal{O}(0.01)$ and correspondingly $\xi \sim 10^4$. If we consider a different RG flow for the self-coupling λ, through the introduction of unknown physics before the inflationary scale, or different boundary conditions at the EW scale, λ will become smaller or larger at inflationary energies. Since, as we will show below, the combination λ/ξ^2 is fixed by the amplitude of the scalar power spectrum, a larger or smaller value of λ during inflation will lead to a correspondingly larger or smaller value of the non-minimal coupling ξ. We will consider values of ξ in the range $10 \leq \xi \leq 10^4$. The inflationary predictions for the scalar and tensor modes for non-minimally coupled models with $\xi \geq 10$ fall into the large-ξ single-field attractor regime, as described for example in Ref. [164]. This results in very simple expressions for the scalar spectral index n_s, the tensor-to-scalar ratio r and the running of the spectral index α as a function of the number of e-folds at horizon-crossing N_*

$$n_s \simeq 1 - \frac{2}{N_*} - \frac{3}{N_*^2}\,, \quad r \simeq \frac{12}{N_*^2}\,, \quad \alpha = \frac{dn_s}{d\ln k} \simeq -\frac{2}{N_*^2}\left(1 + \frac{3}{N_*}\right). \tag{4.34}$$

The values for the spectral observables given in eq. (4.34) correspond to single-field background motion. Multi-field non-minimally coupled models of inflation at large ξ show a very strong single-field attractor behavior. The strength of the attractor was analyzed in Ref. [193] for the case of an $SO(N)$-symmetric model, similar to Higgs inflation without gauge fields. The more general case of two-field inflation with generic potential parameters is given in Refs. [174, 194], showing that the single-field attractor becomes stronger for larger ξ and that it persists not only during inflation but also during the (p)reheating era. For generic initial conditions, the isocurvature fraction $\beta_{\rm iso}$ is exponentially small for random potentials, while for a symmetric potential $\beta_{\rm iso} = \mathcal{O}(10^{-5})$, as is shown in Ref. [194]. As briefly discussed in section 4.4.1 and more extensively in section 5A of Ref. [2], during inflation, the gauge bosons are very massive compared to the Hubble scale, making the single-field attractor behavior of Higgs inflation stronger than the one described in Ref. [193] for

the scalar symmetric case. Hence the use of a single-field motion $\varphi(t)$ for the background is well justified during and after Higgs inflation.

The dimensionless power spectrum of the (scalar) density perturbations is measured to be

$$A_s \simeq 2 \times 10^{-9} \,. \tag{4.35}$$

Using the tensor-to-scalar ratio from eq. (4.34) with $N_* = 55$ yields $r \simeq 3.3 \times 10^{-3}$, and hence the tensor power spectrum becomes

$$\frac{\mathcal{P}_T}{m_{\rm pl}^2} = \frac{2H^2}{\pi^2 m_{\rm pl}^2} = r \times A_s \simeq 6.6 \times 10^{-12} \,. \tag{4.36}$$

Given that the Hubble scale during inflation is approximately [155]

$$H_{\rm infl}^2 \simeq \frac{\lambda}{12\xi^2} m_{\rm pl}^2 \,, \tag{4.37}$$

the Higgs self-coupling and non-minimal coupling must obey the relation

$$\frac{\lambda}{\xi^2} \simeq 5 \times 10^{-10} \,. \tag{4.38}$$

We keep the value of the Hubble scale fixed and determine the value of λ that corresponds to each ξ through eq. (4.38).

4.3 Higgs self-resonance

We now focus on the Higgs fluctuations, neglecting the effects of Goldstone modes and gauge fields. In our linear analysis the Higgs fluctuations do not couple to the gauge field. The equation of motion for the rescaled fluctuations $X^h(x^\mu) \equiv a(t) Q^h(x^\mu)$ is

$$\mathcal{D}_\tau^2 X_{\mathbf{k}}^h + \omega_h^2(k,\tau) X_{\mathbf{k}}^h = 0 \,, \tag{4.39}$$

where the effective frequency is defined as

$$\frac{\omega_h^2(k,\tau)}{a^2} = \frac{k^2}{a^2} + m_{{\rm eff},h}^2 \,. \tag{4.40}$$

For notational simplicity and connection to earlier work [174–176] we define the various contributions to the effective mass of the Higgs fluctuations

$$m^2_{\rm eff,h} \equiv \mathcal{M}^h{}_h - \frac{1}{6}R = m^2_{1,h} + m^2_{2,h} + m^2_{3,h} + m^2_{4,h}\,, \tag{4.41}$$

where $\mathcal{M}^h{}_h$ was defined in eq. (4.19) and

$$\begin{aligned} m^2_{1,h} &= \mathcal{G}^{hh}(\mathcal{D}_\varphi\mathcal{D}_\varphi V)\,, & (4.42)\\ m^2_{2,h} &= -\mathcal{R}^h{}_{LMh}\dot\varphi^L\dot\varphi^M\,, & (4.43)\\ m^2_{3,h} &= -\frac{1}{m^2_{\rm pl}a^3}\mathcal{D}_t\left(\frac{a^3}{H}\dot\varphi^2\mathcal{G}_{hh}\right)\,, & (4.44)\\ m^2_{4,h} &= -\frac{1}{6}R = (\epsilon-2)H^2\,, & (4.45) \end{aligned}$$

where ϵ is the slow-roll parameter $\epsilon = -\dot H/H^2$. For the case of fluctuations along the straight background trajectory, as are Higgs fluctuations, the Riemann contribution $m^2_{2,h}$ vanishes identically. As described in Ref. [36] and further utilized in Ref. [174], the mode-functions can be decomposed using the vielbeins of the field-space metric. In the single-field attractor the decomposition of $X^h_{\mathbf{k}}$ into creation and annihilation operators is trivial

$$\hat X^h = \int \frac{d^3k}{(2\pi)^{3/2}}\left[v_k e_1{}^h\,\hat a_{\mathbf{k}}e^{i\mathbf{k}\cdot\mathbf{x}} + v_k^* e_1{}^h\,\hat a^\dagger_{\mathbf{k}}e^{-i\mathbf{k}\cdot\mathbf{x}}\right]\,, \tag{4.46}$$

where $e_1{}^h = \sqrt{\mathcal{G}^{hh}}$. Since the vielbeins obey the parallel transport equation $\mathcal{D}_\tau e_1{}^h = 0$, the equation of motion for the mode function $v_{\mathbf{k}}$ becomes

$$\partial^2_\tau v_{\mathbf{k}} + \omega^2_h(k,\tau)v_{\mathbf{k}} = 0\,. \tag{4.47}$$

We solve the equation in cosmic, rather than conformal time, which is better suited for computations after inflation

$$\ddot v_{\mathbf{k}} + H\dot v_{\mathbf{k}} + \frac{\omega^2_h(k,t)}{a^2}v_{\mathbf{k}} = 0\,, \tag{4.48}$$

where the frequency is defined in eq. (4.40).

We examine the two dominant terms of the effective mass, the one arising from the potential ($m^2_{1,h}$) and the one arising from the coupled metric perturbations ($m^2_{3,h}$). The latter is often overlooked in studies of preheating, perhaps because it is vastly subdominant during inflation. It arises by combining the equation of motion for $\delta\phi$ and the metric perturbation ψ, defined through eq. (4.12),

in conjunction with the definition of the Mukhanov-Sasaki variables, given in eq. (4.14).

The expression for $m_{1,h}^2$ normalized by the Hubble scale is

$$\begin{aligned}\frac{m_{1,h}^2}{H^2(t)} =& \frac{12m_{\rm pl}^2\left(\xi\varphi^2\left(12\xi m_{\rm pl}^2 - 2\xi(6\xi+1)\varphi^2 + m_{\rm pl}^2\right) + 3m_{\rm pl}^4\right)}{\varphi^2\left(\xi(6\xi+1)\varphi^2 + m_{\rm pl}^2\right)^2} \\ \simeq& -\frac{4m_{\rm pl}^2}{\xi\varphi^2} + \frac{4m_{\rm pl}^4}{\xi^2\varphi^4} + \mathcal{O}\left(\frac{m_{\rm pl}^6}{\xi^3\varphi^6}\right),\end{aligned} \tag{4.49}$$

where we used $\xi \gg 1$ in expressions such as $(6\xi + 1) \simeq 6\xi$. Furthermore, since we are at first interested in studying the behavior during inflation, where analytic progress can be made, we use $\xi\varphi^2 \gg m_{\rm pl}^2$ as an approximation. As we will see, this works reasonably well even close to the end of inflation. We can use the single-field slow-roll results

$$-N = \frac{3}{4}\frac{\xi\varphi^2}{m_{\rm pl}^2} + \frac{1}{8}\frac{\varphi^2}{m_{\rm pl}^2} + \mathcal{O}\left(\log\frac{\varphi}{m_{\rm pl}}\right), \tag{4.50}$$

where we went beyond lowest order in $\xi\varphi^2$ and we measure the number of e-folds from the end of inflation, meaning that negative values correspond to the inflationary era[5]. This leads to

$$\frac{m_{1,h}^2}{H^2(t)} \simeq \frac{3}{N} + \frac{9}{4N^2} + \mathcal{O}\left(\frac{1}{N^3}\right). \tag{4.51}$$

If we minimize m_1^2 as a function of $\delta = \sqrt{\xi}\varphi$, the field amplitude that minimizes the mass is

$$\delta_{\rm min} = \sqrt{2}m_{\rm pl} + \mathcal{O}\left(\frac{1}{\xi}m_{\rm pl}\right), \tag{4.52}$$

or equivalently $N_{\rm min} \simeq -1.5$. For the minimization we used the full expression for the effective mass and only took the Taylor expansion for large ξ at the end. We can see that, for $\xi \gg 1$ the minimum of m_1^2 is independent of ξ and thus occurs at the same value of δ, which will also be the same value of N, in the approximation of eq. (4.50). In general, the function $m_{1,h}^2(N)/H^2$ shows no appreciable difference for different values of $\xi \gg 1$ during inflation. This can be easily seen by substituting eq. (4.50) into eq. (4.49). As shown in Ref. [175], this behavior persists during the time of coherent inflaton oscillations.

[5]We neglected the contributions coming from the lower end of the integral leading to eq. (4.50).

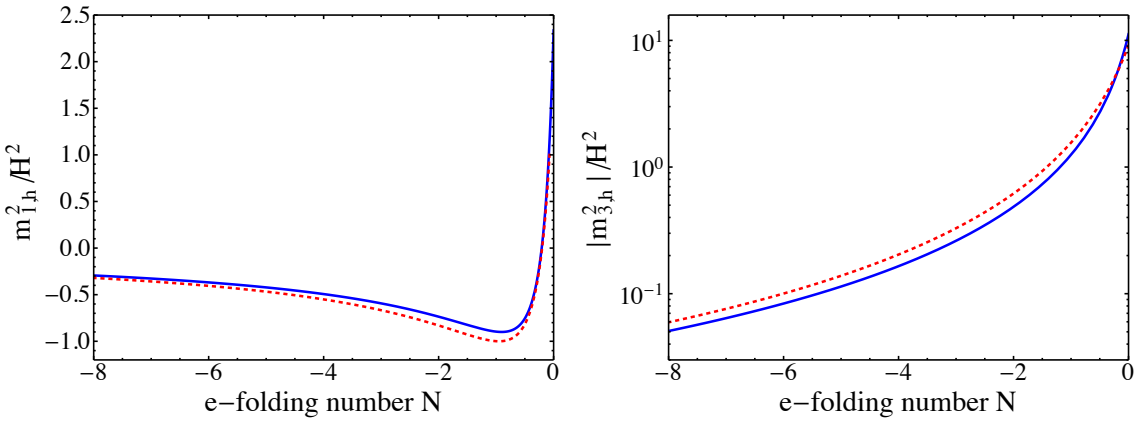

FIGURE 4.1: The components of the effective mass of the Higgs fluctuations $m^2_{1,h}$ and $m^2_{3,h}$ rescaled by the Hubble scale. The blue curves show the numerical curves for $\xi = 10$ and the red dashed lines the approximate analytic expressions of eqs. (4.51) and (4.54) respectively.

The mass component arising from the metric fluctuations is

$$m^2_{3,h} = -\frac{\left(\xi(6\xi+1)\varphi^2 + m^2_{\rm pl}\right)\dot{\varphi}\left(H(t)(\epsilon(t)+3)\dot{\varphi} + 2\ddot{\varphi}\right)}{H(t)\left(\xi\varphi^2 + m^2_{\rm pl}\right)^2} \simeq -\frac{18\dot{\varphi}^2}{\varphi^2}\,, \tag{4.53}$$

where the last approximation holds during inflation. Using the slow-roll expression for $\dot{\varphi}$ we get that during inflation

$$\frac{m^2_{3,h}}{H^2(t)} \simeq -\frac{9}{2N^2}\,. \tag{4.54}$$

This contribution is clearly subdominant to $m^2_{1,h}$, hence it can be safely neglected during inflation. However, $|m^2_{3,h}|$ grows near the end of inflation, since it is proportional to $\dot{\varphi}^2$, which at the end of inflation is given by

$$\dot{\varphi}^2_{\rm end} = \mathcal{G}^{\varphi\varphi}V = \frac{\lambda m^2_{\rm pl}\varphi^4}{4\left(6\xi^2\varphi^2 + \xi\varphi^2 + m^2_{\rm pl}\right)} \simeq \frac{\lambda m^2_{\rm pl}\varphi^2}{24\xi^2}\,. \tag{4.55}$$

It has been numerically shown in Ref. [174] that the field value at the end of inflation is $\sqrt{\xi}\varphi_{\rm end} \simeq 0.8 m_{\rm pl}$, leading to

$$\dot{\varphi}^2_{\rm end} \simeq \frac{0.8^2\lambda}{24\xi^3} m^4_{\rm pl} \simeq \frac{2\lambda}{75\xi^3} m^4_{\rm pl}\,. \tag{4.56}$$

Numerically we get $m^2_{3,h}/H^2(t) \simeq -11$ at the end of inflation, in rough agreement with the approximate expressions given above.

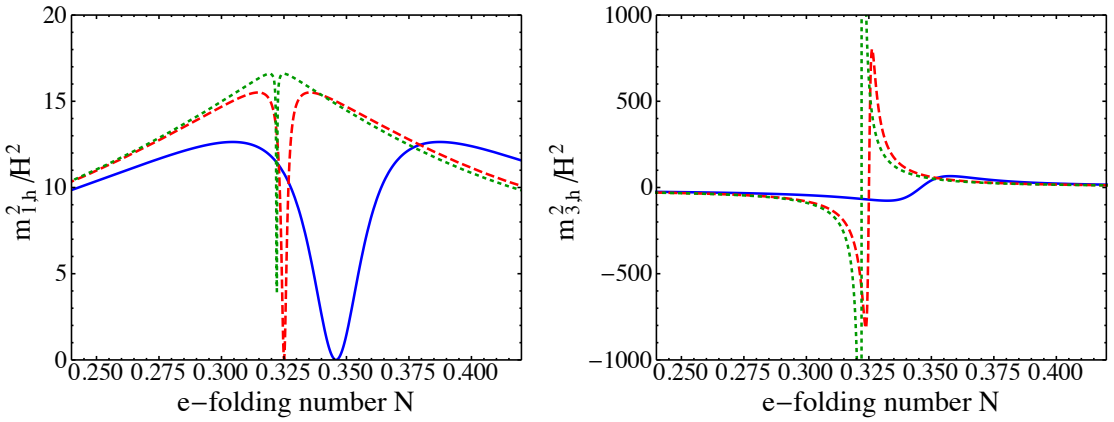

FIGURE 4.2: The ratio of the components of the effective mass of the Higgs fluctuations $m^2_{1,h}$ (left) and $m^2_{3,h}$ (right) rescaled by the Hubble scale at the end of inflation. The blue, red dashed and green dotted curves correspond to $\xi = 10, 10^2, 10^3$ respectively.

The numerical results for $\xi = 10$ are shown in figure 4.1, along with the approximate analytical expressions that we derived. We only show the $\xi = 10$ case, since all cases with higher values of the non-minimal coupling exhibit visually identical results. After the end of inflation the two dominant components of the effective mass of the Higgs fluctuations evolve differently for different values of ξ. In Ref. [175] the behavior of $m^2_{1,h}$ was analyzed in the static universe approximation. It was shown that for $\xi \gtrsim 100$ the effective mass component $m^2_{1,h}$ quickly approaches a uniform shape regardless of the value of ξ. The consequence of that is that the Floquet chart for the inflaton self-resonance also approaches a common form for $\xi \gtrsim 100$. This can be seen in the left panel of figure 4.2, where $m^2_{1,h}$ is very similar between $\xi = 100$ and $\xi = 10^3$, but different for $\xi = 10$. The coupled metric fluctuations component of the effective mass has a similar shape for $\xi = 100$ and $\xi = 10^3$, but for $\xi = 10$ it is significantly less pronounced, as seen in the right panel of figure 4.2.

4.3.1 Superhorizon evolution and thermalization

An important notion when dealing with (p)reheating is the transfer of energy from the inflaton condensate to the radiation degrees of freedom. Naively, one must compute all the power concentrated in the wave numbers that are excited above the vacuum energy (different than the adiabatic vacuum at any time) and compare that to the energy density stored in the condensate. However, when dealing with inflationary perturbations, one must keep in mind that computations should refer to modes, whose length-scales are relevant to the dynamics being studied. For curvature perturbations,

the use of a finite box was described in Ref. [198]. For preheating, since thermalization proceeds through particle interactions, the relevant length-scales are those that allow for particle interactions, hence subhorizon scales, or short wavelengths.

The parametric excitation of long-wavelength modes has been extensively studied [83, 199–207]. It has been demonstrated that the coupled metric fluctuations lead to an enhancement of –particularly– long-wavelength modes [200, 202, 203, 205, 207], which is larger than the one computed using a rigid background. Furthermore, the amplification of long-wavelength modes, even on super Hubble scales, does not violate causality, as discussed for example in Refs. [199, 200, 202, 203, 207]. Intuitively, the inflaton condensate has a super-Hubble correlation length and can thus consistently affect super-Hubble modes.

While UV modes encounter the complication of possibly being excited for wavenumbers that exceed the unitarity bound (this doesn't occur for Higgs modes), the IR modes have a different conceptual difficulty: since thermalization occurs when particles interact and exchange energy, in order to lead to a thermal distribution, modes that are superhorizon are 'frozen-in' and hence cannot take part in such processes[6]. Hence, it is normal to only consider modes that have large enough physical wave numbers, that place them inside the horizon at the instant in time that we are considering. Modes that have longer wavelengths are frozen outside the horizon and do not contribute to the thermalization process. They should be summed over and added to the local background energy density. We will skip this last step, as their contribution is subdominant, compared to the energy density stored in the inflaton condensate. In figure 4.3 we see the evolution of the comoving Hubble radius, that is determined from the background field φ, neglecting any backreaction from decay products. The Hubble radius shrinks during inflation and grows after inflation ends. We also see that different values of ξ lead to different post-inflationary evolution, which is expected, since the effective equation of state of the background dynamics after inflation depends strongly on ξ, as shown in Ref. [174]. More specifically, large non-minimal couplings $\xi \gtrsim 100$ lead to a prolonged period of matter-domination-like expansion, which can last for several e-folds in the absence of backreaction. As we will see in the next sections, the majority of the parametric resonance effects occur for $N \lesssim 3$ e-folds, placing the entirety of the reheating dynamics inside the matter-dominated background era for large values of ξ. In order to take into account the relevant wavenumbers consistently, we use an

[6]Generically in multi-field models, one would not expect the curvature perturbations to remain frozen in when stretched outside the Hubble radius, since multi-field interactions can generate non-adiabatic pressure, which in turn will source changes in the gauge-invariant curvature perturbations on arbitrarily long length-scales. However, in models like Higgs inflation that feature strong single-field attractor dynamics during inflation, the non-adiabatic pressure effectively vanishes and the long-wavelength modes remain frozen in, akin to the expected behavior in simple single-field models. Details on the single-field attractor in such models can be found in Refs. [164, 174, 193].

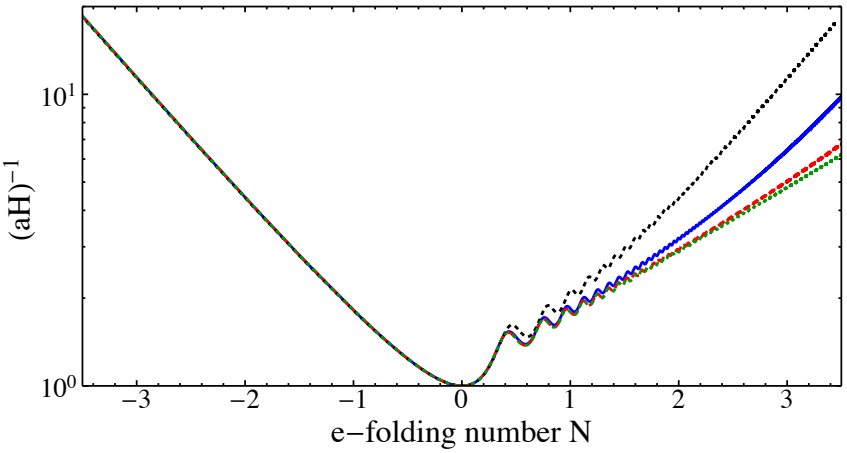

FIGURE 4.3: The size of the comoving Hubble radius during and after inflation for $\xi = 10, 10^2, 10^3, 10^4$ (black, blue, red and green respectively). The curves are normalized such that $(aH)^{-1} = 1$ at the end of inflation.

adaptive code, that only sums up the contribution of modes that are inside the horizon at the point in time when computing the energy density of the Higgs field fluctuations.

4.3.2 Preheating

We now move to the computation of the energy density in the Higgs particles that are produced during preheating, for which we solve eq. (4.40) numerically. Again we use cosmic time rather than conformal time. A detailed analysis was already performed in Ref. [176]. However, all computations were initialized at the end of inflation, thereby neglecting the amplification of long-wavelength modes during the last e-folds of inflation. We initialize all computations at 4.5 e-folds before the end of inflation, in order to ensure that all relevant modes are well described by the Bunch-Davies (BD) vacuum solution

$$v_{k,h} \simeq \frac{1}{\sqrt{2k}} e^{-ik\tau} \,. \tag{4.57}$$

We see in the right panel of figure 4.4 that at early times (before the end of inflation), the energy density in Higgs modes (indicated by the solid blue line) decays as a^{-4} (indicated by the dotted line), in keeping with the expectation for modes in the BD state. However, approximately one e-fold before the end of inflation, the evolution of the energy density in Higgs modes departs from a^{-4}, because the low k-modes are enhanced with respect to the BD spectrum. This enhancement occurs

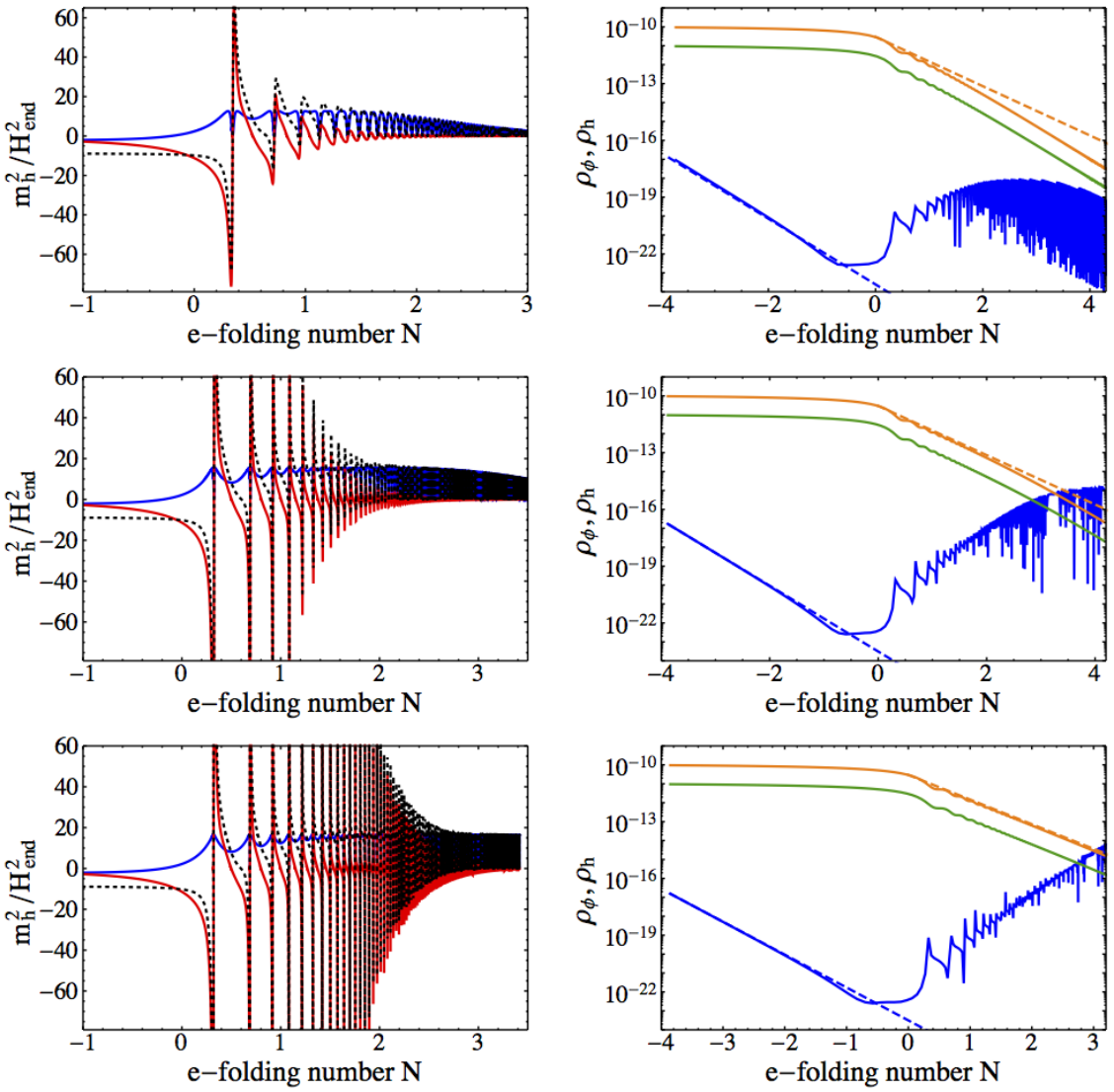

FIGURE 4.4: *Left:* The effective mass-squared (black-dotted), along with the contributions from the potential (blue) and the coupled metric perturbations (red).
Right: The energy density in the background Higgs condensate (orange) and the Higgs fluctuations (blue) for $\xi = 10, 10^2, 10^3$ (top to bottom) in units of $m_{\rm pl}^4$. The green line shows 10% of the background energy density, which is used as a proxy for the limit of our linear analysis. The orange-dashed line is $\rho_0 a^{-4}$, corresponding to the red-shifting of the background energy density during radiation-dominated expansion.

because $m_{{\rm eff},h}^2 < 0$, an early tachyonic amplification phase driven largely by the effect of coupled metric perturbations. An immediate consequence of this fact is that one would underestimate the true amount of growth by starting the computation in a BD-like vacuum state at the end of inflation.

The right panels of figure 4.4 present the results for the energy transfer into Higgs particles for $\xi = 10, 10^2, 10^3$. Preheating completes when the energy density in the Higgs fluctuations (blue line) becomes equal to the energy density of the background field (orange line). However, the linear analysis is expected to break down when the energy density of the Higgs fluctuations becomes comparable to that of the inflaton field. As an indicator of the validity of the linear theory, which neglects backreaction of the excited modes onto the background, the green line shows 10% of the energy density of the inflation field.

For all values of ξ studied, the system exhibits an amplification of inflaton (Higgs) fluctuations. This is mainly caused by the periodic negative contribution of $m^2_{3,h}$ to the effective mass-squared $m^2_{\text{eff},h}$, which is plotted in the left panel of figure 4.4. This is the term arising from considering the effect of the coupled metric perturbations at linear order. As shown in Ref. [176] and further reiterated in figure 4.4, the amplification driven by $m^2_{3,h}$ lasts longer for larger values of ξ. Specifically, the time at which the tachyonic resonance regime stops scales as $t \sim \sqrt{\xi} H^{-1}_{\text{end}}$, as shown in Ref. [176]. However, for $\xi > 100$ the differences are irrelevant (in the simplified linear treatment), since the universe will have preheated already by $N \simeq 3$ e-folds. Hence for $\xi > 100$, self-resonance of the Higgs field leads to predictions for the duration of preheating that are almost independent of the exact value of ξ.

After the tachyonic resonance has shut off (and if preheating has not completed yet), the modes undergo parametric resonance, driven by the oscillating effective mass term $m^2_{1,h}$. However, for very long-wavelength modes $k \simeq 0$, the Floquet exponent vanishes [175], and the amplification is polynomial in time rather than exponential, hence significantly weaker. As shown in Ref. [175] the maximum Floquet exponent in the static universe approximation is $\mu_{k,\max} T \approx 0.3$, where T is the background period. Using the relation $\omega/H \simeq 4$, which was derived in Ref. [174] for $\omega = 2\pi/T$, the maximum Floquet exponent is expressed as $\mu_k \sim 0.5H$. Hence the Floquet exponent is too small to lead to an efficient amplification of Higgs fluctuations in an expanding universe. Thus the early time tachyonic resonance, driven by the coupled metric fluctuation is crucial for preheating the universe through Higgs particle production.

For $\xi = 10$ the situation is significantly different. Both tachyonic resonance, due to the coupled metric fluctuations encoded in $m^2_{3,h}$, as well as parametric resonance due to the potential term $m^2_{1,h}$ become inefficient earlier, leading to a slower growth of the fluctuations and the energy density that they carry and an incomplete preheating.

However, for smaller values of the non-minimal coupling $\xi = \mathcal{O}(10)$ one must take into account another important feature, namely the evolution of the background. As shown in Ref. [174], larger

values of ξ put the universe into a prolonged matter-dominated state ($w = 0$). This means that the energy density of the background condensate redshifts as $a^{-3} = e^{-3N}$. For small values of ξ, however, the universe passes briefly through the background (average) equation of state $w = 0$ and after the first e-fold approaches $w \simeq 1/3$. Figure 4.5 shows the evolution of the energy density in Higgs modes for the marginal case of $\xi = 30$. We see that the fluctuation energy density in the Higgs modes would be always smaller than the background, if the background evolved with $w \simeq 0$, as indicated by the orange dashed line. However, the fact that the background energy density redshifts faster ($w \simeq 1/3$) allows for complete preheating. Simply put, non-minimal couplings in the 'intermediate' regime of $\xi = \mathcal{O}(10)$ exhibit a shorter period of tachyonic-parametric amplification, while at the same time following a background evolution of $\rho_\phi \sim e^{-4N}$.

We distinguish two time points relevant for preheating: $N_{\rm reh}$ is the time at which the energy density in the linear fluctuations equals the background energy density, which we take as the time of complete preheating and $N_{\rm br}$ is the time at which the energy density in the linear fluctuations equals 10% of the background energy density, which is the point at which backreaction effects may become important. We have numerically found that self-resonance of the Higgs field becomes insufficient to preheat the universe at $\xi < 30$. In particular, the results for $N_{\rm reh}(\xi)$ can be fitted by a simple analytical function, as shown in figure 4.6:

$$N_{\rm reh}(\xi) \simeq \frac{21}{\xi(1 + 0.016\xi)} + 3\,, \tag{4.58}$$

for $\xi \gtrsim 30$, where complete preheating is possible, at least in the linear approximation that we use. For $\xi > 100$, $N_{\rm reh}$ becomes largely independent of ξ, as expected from the results of figure 4.4. As a final note, we must say that the results were insensitive to the exact value of the maximum wavenumber considered. This is due to the fact that the small (but subhorizon) wavenumbers $k = \mathcal{O}(H_{\rm end})$ are exponentially amplified and dominate the fluctuation energy density shortly after the end of inflation. Hence we do not need to implement any scheme to subtract the vacuum contribution from large-k modes, since it is vastly subdominant for any reasonable UV cutoff.

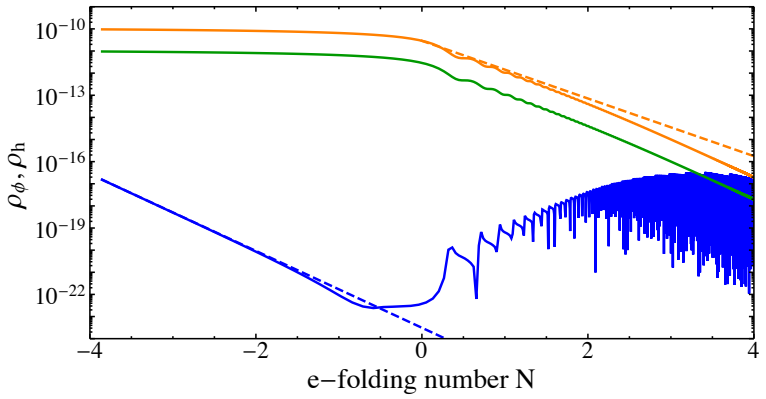

FIGURE 4.5: The energy density in the background Higgs condensate (orange) and the Higgs fluctuations (blue) for the marginal case of $\xi = 30$ (top to bottom) in units of $m_{\rm pl}^4$. The green line shows 10% of the background energy density, which is used as a proxy for the limit of our linear analysis. The orange-dashed line is $\rho_0 a^{-4}$, corresponding to the red-shifting of the background energy density during radiation-dominated expansion.

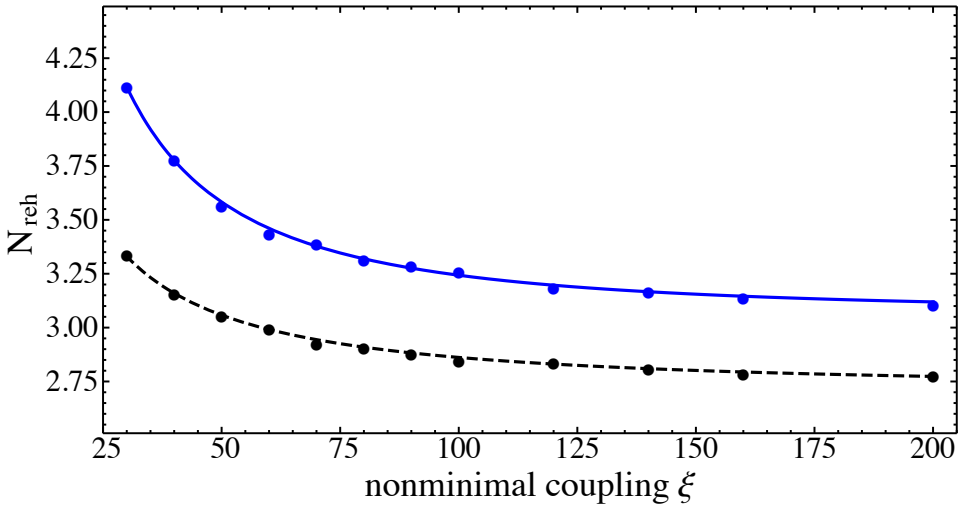

FIGURE 4.6: The number of e-folds after inflation when the energy density in the Higgs fluctuations equals the background energy density $N_{\rm reh}$ (blue solid) or 10% of the background energy density $N_{\rm br}$ (black dashed).

4.4 Gauge / Goldstone boson production

4.4.1 Initial conditions for preheating

In section 5A of Ref. [2] we use the equations of motion derived in the Abelian model in unitary gauge, in order to study the evolution of gauge fields during inflation. The unitary gauge is well-defined in this period, since $\varphi(t)$ does not vanish. The values of $B_{\mathbf{k}}^{\pm,L}$ at the end of inflation, when $t = t_{\rm in}$, serve as initial conditions for preheating. Especially for initializing lattice simulations, which are increasingly expensive to start deeper within inflation, accurate knowledge of the spectrum of gauge fields at the end of inflation is essential. During preheating, unitary gauge is not well-defined at moments when $\varphi(t) = 0$, so we use Coulomb gauge. In order to determine the initial condition for $\theta_{\mathbf{k}}$, we will use eq. (4.32), which relates $B_{\mathbf{k}}^{L}$ in unitary gauge to $\theta_{\mathbf{k}}$ in Coulomb gauge.

During inflation we find that the transverse modes are canonically normalized and conformally coupled at early times and the modes therefore follow the Bunch-Davies vacuum solution. At late times they become heavy and thus suppressed. The longitudinal gauge modes are of greater interest, since they will be amplified during preheating. It turns out that they follow the adiabatic WKB-solution until the end of inflation. The longitudinal modes are very heavy during inflation (as compared to the Hubble scale). This enhances the single-field attractor behavior.

Using eq. (4.32) to translate the solution for the longitudinal mode in unitary gauge to the Goldstone mode in Coulomb gauge, we find

$$\theta_{\mathbf{k}}(t_{\rm in}) = \frac{1}{\sqrt{2}} \frac{e\varphi(t_{\rm in})}{k} \frac{1}{\sqrt{b_L(k,t_{\rm in})}\sqrt{\omega_L(k,t_{\rm in})}}\,, \tag{4.59}$$

$$\dot{\theta}_{\mathbf{k}}(t_{\rm in}) = -i\,\frac{\omega_L(k,t_{\rm in})}{a(t_{\rm in})} \times \theta_k(t_{\rm in}) \tag{4.60}$$

with

$$b_L(k,\tau) = \left(1 + \frac{k^2 2f}{m_{\rm pl}^2 a^2 e^2 \varphi^2}\right)\,, \qquad \omega_L^2(k,\tau) = k^2 + a^2 \frac{m_{\rm pl}^2}{2f} e^2 \varphi^2\,. \tag{4.61}$$

If we focus on the case of $k|\tau| \gg \sqrt{\frac{12\xi}{\lambda}} e \equiv x_c$, where the initial conditions for preheating are

$$\theta_{\mathbf{k}}(\tau_{\rm in}) \approx \frac{e\phi}{x_c} \frac{\tau_{\rm in}}{\sqrt{2k}}\,, \tag{4.62}$$

$$\dot{\theta}_{\mathbf{k}}(\tau_{\rm in}) \approx \theta_{\mathbf{k}}(\tau_{\rm in}) \times \left(\frac{i\,k}{a(\tau_{\rm in})}\right)\,, \tag{4.63}$$

we find that for large wavenumbers the coupling constant e drops out of the initial conditions for the θ field (since $x_c \propto e$), hence the decoupling limit is trivially obtained. For $k|\tau| < x_c$ it is slightly more complicated to see that, since for $e \to 0$ we get $x_c \to 0$, hence that region shrinks into nonexistence as we take the decoupling limit. Also, we would have to compute the expressions for $x_c \ll 1$ before we send $e \to 0$ in that case. Since the case of $e \ll 1$ does not apply to Higgs inflation, we will not pursue it further.

4.4.2 Preheating

We start by rewriting eq. (4.29) in a somewhat more compact way

$$\begin{aligned} &\mathcal{D}_\tau^2 X^\theta - \partial_\tau \log\left(1+\frac{\tilde{m}_B^2}{k^2}\right)\mathcal{D}_\tau X^\theta \\ &\quad + \left[k^2 + a^2 m_{\mathrm{eff},\theta}^2 + \tilde{m}_B^2 + \left(\frac{\partial_\tau \varphi}{\varphi} + \frac{\partial_\tau a}{a} - \frac{\partial_\tau f}{2f}\right)\partial_\tau \log\left(1+\frac{\tilde{m}_B^2}{k^2}\right)\right] X^\theta = 0\,, \end{aligned} \tag{4.64}$$

where we defined the gauge field mass

$$\tilde{m}_B^2 \equiv e^2\varphi^2 \frac{m_{\mathrm{pl}}^2}{2f} a^2\,, \tag{4.65}$$

and $X^\theta = a(t)\cdot\theta$. We normalize the scale factor as $a = 1$ at the end of inflation. The effective mass of the Goldstone mode θ in the absence of gauge fields is

$$m_{\mathrm{eff},\theta}^2 \equiv \mathcal{M}^\theta{}_\theta - \frac{1}{6}R = m_{1,\theta}^2 + m_{2,\theta}^2 + m_{3,\theta}^2 + m_{4,\theta}^2\,, \tag{4.66}$$

with

$$m_{1,\theta}^2 = \mathcal{G}^{\theta\theta}(\mathcal{D}_\theta\mathcal{D}_\theta V)\,, \tag{4.67}$$

$$m_{2,\theta}^2 = -\mathcal{R}^\theta{}_{hh\theta}\,\dot{\varphi}^2\,, \tag{4.68}$$

$$m_{3,\theta}^2 = 0, \tag{4.69}$$

$$m_{4,\theta}^2 = -\frac{1}{6}R = (\epsilon - 2)H^2\,. \tag{4.70}$$

The numerical solution of eq. (4.64) was again performed in cosmic rather than conformal time and the computations were initialized at the end of inflation, according to eq. (4.59) and eq. (4.60).

We can follow the quantization method described in Ref. [174] and utilized in section 4.3 for the study of Higgs self-resonance:

$$\hat{X}^\theta = \int \frac{d^3k}{(2\pi)^{3/2}} \left[z_k e_2{}^\theta \, \hat{a}_{\mathbf{k}} e^{i\mathbf{k}\cdot\mathbf{x}} + z_k^* e_2{}^\theta \, \hat{a}_{\mathbf{k}}^\dagger e^{-i\mathbf{k}\cdot\mathbf{x}} \right] , \tag{4.71}$$

where $e_2{}^\theta = \sqrt{\mathcal{G}^{\theta\theta}}$. Using the vielbein decomposition again, the covariant derivatives are effectively substituted by partial ones

$$\begin{aligned} &\partial_\tau^2 z_k - \partial_\tau \log(1+\tilde{m}_B^2/k^2) \cdot \partial_\tau z_k \\ &\quad + \left(k^2 + a^2 m_{\mathrm{eff},\theta}^2 + \tilde{m}_B^2 + \frac{1}{2}\partial_\tau \log\left(\tilde{m}_B^2 \sqrt{\frac{2f}{m_{\mathrm{pl}}^2}} \right) \partial_\tau \log\left(1 + \frac{\tilde{m}_B^2}{k^2} \right) \right) z_k = 0 \, . \end{aligned} \tag{4.72}$$

In order to eliminate the first-derivative term we can use the rescaled variable $\tilde{z}_k$, defined as

$$z_k = \sqrt{1 + \frac{\tilde{m}_B^2}{k^2}} \, \tilde{z}_k \equiv T \cdot \tilde{z}_k \, , \tag{4.73}$$

leading to

$$\partial_\tau^2 \tilde{z}_k + \omega_z^2 \, \tilde{z}_k = 0 \, , \tag{4.74}$$

where

$$\omega_z^2 = k^2 + a^2 m_{\mathrm{eff},\theta}^2 + \tilde{m}_B^2 + \frac{1}{2}\partial_\tau \log\left(\tilde{m}_B^2 \sqrt{\frac{2f}{m_{\mathrm{pl}}^2}} \right) \partial_\tau \log(T^2) + \frac{\partial_\tau^2(\tilde{m}_B^2)}{2k^2T^2} - \frac{3}{4}\frac{(\partial_\tau \tilde{m}_B^2)^2}{k^4 T^4} \, , \tag{4.75}$$

where $\tilde{m}_B^2$ is larger than $m_{1,\theta}^2$ and $m_{4,\theta}^2$. As discussed extensively in Refs. [174–176] for the case of a purely scalar multi-field model with large non-minimal couplings to gravity, the field-space manifold is asymptotically flat for large field values and exhibits a curvature 'spike' at the origin $\varphi(t) \simeq 0$. This 'Riemann spike' is exhibited in the effective mass of the isocurvature modes $m_{\mathrm{eff},\theta}^2$, more specifically in the $m_{2,\theta}^2$ component, which is subdominant for all times away from the zero-crossings of the background value of the inflaton field $\varphi(t)$. We will not reproduce the entirety of the Floquet structure of this model, both because we do not wish to repeat the analysis of [175], and because, as we will see in the subsequent section, the first zero-crossing of $\varphi(t)$ is the only relevant one for preheating through gauge modes.

In order to estimate the maximum excited wavenumber k_{max}, we consider the following approximation, containing only the dominant terms

$$\omega_{z,\,\mathrm{approx}}^2 \equiv k^2 + a^2 m_{2,\theta}^2 + \tilde{m}_B^2 \, , \tag{4.76}$$

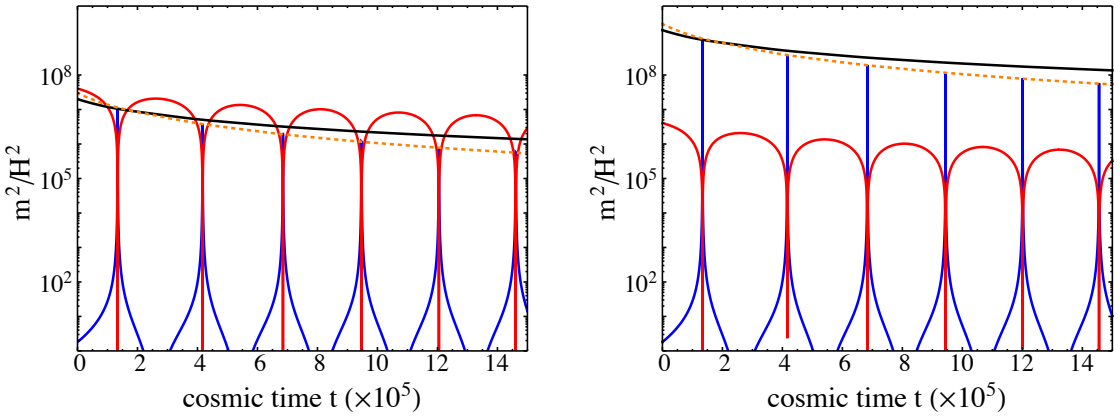

FIGURE 4.7: Dominant components of the effective frequency-squared for $\xi = 10^3$ (left) and $\xi = 10^4$ (right). Color coding is as follows: $\tilde{m}_B^2/a^2$ (red), $m_{2,\theta}^2$ (blue) and k^2/a^2 (black) for the maximum excited wavenumber $k_{\rm max}$. The orange-dotted curve shows the scaling a^{-3}.

where $\tilde{m}_B^2$ dominates over all subsequent terms in eq. (4.75) for large k. Figure 4.7 shows the three contributions to $\omega_{z,\,\rm approx}^2$ for $\xi = 10^3, 10^4$ for $k = k_{\rm max}$. As shown in Ref. [176], the scaling of the spike in the effective mass is

$$\frac{m_{2,\theta}^2\Big|_{\rm max}}{\langle H(t)\rangle^2} = \mathcal{O}(10)\xi^2\,, \tag{4.77}$$

where $\langle H(t)\rangle$ is a time-averaged version of the Hubble scale over the early oscillatory behavior. The range of excited wavenumbers is given by the relation

$$k^2 \lesssim a^2\, m_{2,\theta}^2\big|_{\rm max}\,, \tag{4.78}$$

assuming that the spike of $m_{2,\theta}^2$ dominates over $\tilde{m}_B^2$ near $\varphi(t) = 0$. Each subsequent inflaton zero-crossing affects a smaller range of wavenumbers, since $m_{2,\theta}^2 \propto H^2 \propto \rho_{\rm infl.} \propto a^{-3}$, where we assumed $w = 0$ for the averaged background evolution. Altogether $k_{\rm max}^2 \propto a^{-1}$, hence the maximum excited wavenumber shrinks for every subsequent inflaton oscillation. The maximum comoving wavenumber after the first inflaton zero-crossing, where $a(t) \approx 1$, is

$$k_{\rm max}^2 = \mathcal{O}(10)\xi^2 H_{\rm end}^2 = \mathcal{O}(1)\lambda\, m_{\rm pl}^2\,, \tag{4.79}$$

where we used eq. (4.37) and $H_{\rm end} \approx 0.5 H_{\rm infl}$. This is in agreement with Ref. [177]. We focus primarily on the first inflaton zero-crossing, since the produced gauge bosons will decay into fermions between two subsequent background zero-crossings, hence Bose enhancement is lost. This was shown

in Refs. [171, 172] and will be discussed in section 4.5.

The second dominant component of the gauge field effective frequency-squared is $\tilde{m}_B^2$, which scales simply as

$$\frac{\tilde{m}_B^2/a^2}{H_{\rm end}^2} = \frac{m_{\rm pl}^2 e^2}{2f}\varphi^2 \frac{1}{H_{\rm end}^2} = \mathcal{O}(1)\frac{\xi}{\lambda} = \mathcal{O}(1)\frac{10^{10}}{\xi}\,, \tag{4.80}$$

where the $\lambda - \xi$ relation given in eq. (4.38) was used at the last step. We can see that for $\xi = 10^3$ the maxima of the two contributions $\tilde{m}_B^2$ and $m_{2,\theta}^3$ are similar, as shown in figure 4.7 .

Computing the energy density transferred from the inflaton condensate into the gauge field modes requires more attention than the corresponding computation of section 4.3 for the Higgs self-resonance. In the case of Higgs self-resonance, the range of excited wavenumbers is $k_{\rm max}^h \sim H$. A naive computation of the energy density in the local adiabatic (WKB) vacuum for the same modes gives $\rho_{BD} \sim k_{\rm max}^4 \sim H^4$ which is 10 orders of magnitude smaller than the background energy density[7]. In that case we do not need to subtract this unphysical vacuum contribution from the energy density of the Higgs modes, since the energy density in the parametrically amplified modes is exponentially larger.

For the case of gauge fields the maximum wavenumber up to which modes can be excited is given in eq. (4.79). The vacuum energy density in these modes, naively computed, is $\rho_{\rm BD} \sim k_{\rm max}^4 \sim \lambda^2 m_{\rm pl}^4$. The total energy density in the inflaton field is $\rho_{\rm infl} = 3H^2 m_{\rm pl}^2$ leading to $\rho_{\rm BD}/\rho_{\rm infl} \sim \lambda\,\xi^2 \sim 10^{-10}\xi^4$. This is much greater than unity for large values of the non-minimal coupling. We thus need to remove the unphysical vacuum contribution to the energy density using the adiabatic subtraction scheme [135]. In this scheme we compare the wave-function of the gauge fields to the instantaneous adiabatic vacuum, computed in the WKB approximation, isolating the particle number for each wavenumber k. The particle number corresponding to a mode v_k is given by:

$$n_k = \frac{\omega_k}{2}\left(\frac{|\dot{v}_k|^2}{\omega_k^2} + |v_k|^2\right) - \frac{1}{2}\,. \tag{4.81}$$

A drawback of this method is that the particle number is only well-defined when the adiabaticity condition holds $\dot{\omega}_k/\omega_k^2 \ll 1$, thus we cannot define the particle number in the vicinity of the Riemann spike, when $\varphi(t) = 0$[8].

[7] Any computation that does not involve vacuum subtraction, including lattice simulations such as Refs. [208, 209], deals with classical quantities and computes the energy density of the vacuum modes as if they were physical. Such a computation is valid as long as the unphysical energy density of the vacuum modes is vastly subdominant.

[8] Ref. [177] computed the particle number, working in the Jordan frame, arriving at similar results. The energy of the gauge fields was subsequently computed using the value of the gauge field mass directly on the Riemann spike. We refrain from using $m_{2,\theta}^2\big|_{\rm max}$ as an indicator of the gauge field mass, since the particle number is not a well-defined

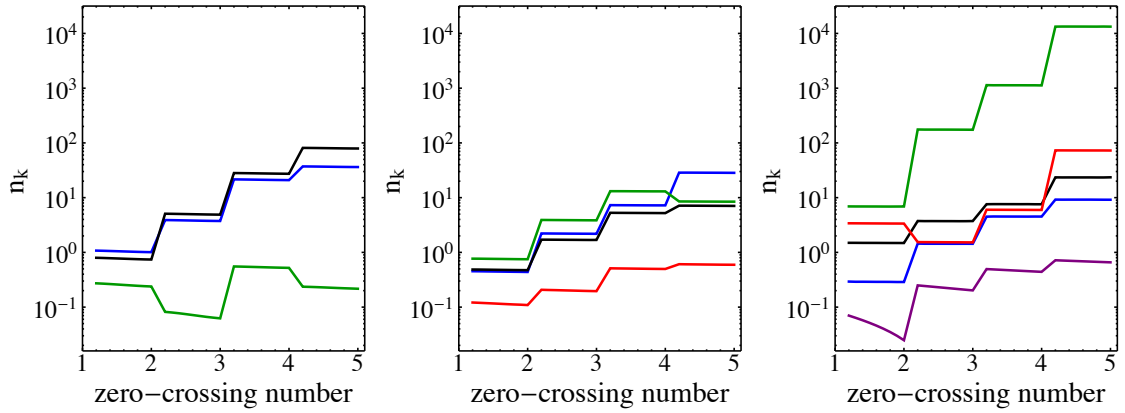

FIGURE 4.8: The particle number density for $k/H_{\rm end} = 1, 150, 550, 2600, 28000$ (blue, black, green, red and purple respectively). From left to right: $\xi = 10^2, 10^3, 10^4$. If a colored curve is missing from a panel, the corresponding wavenumber is not excited.

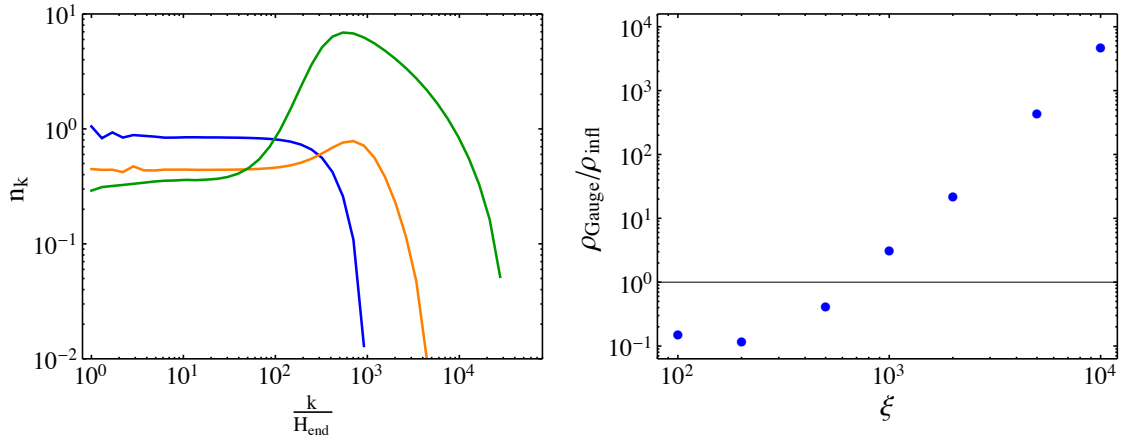

FIGURE 4.9: Left: The particle number density after the first inflaton zero-crossing for $\xi = 10^2, 10^3, 10^4$ (blue, orange and green respectively)
Right: The ratio of the energy density in gauge fields to the background inflaton energy density as a function of the non-minimal coupling ξ after the first zero-crossing. We see that for $\xi \gtrsim 10^3$ gauge boson production can preheat the universe after one background inflaton zero-crossing, hence it is much more efficient than Higgs self-resonance.

The energy density is easily computed through the particle number as

$$\rho^{L,\theta} = \int \frac{d^3k}{(2\pi)^3} n_k \omega_k \,. \tag{4.82}$$

quantity there. For $\xi \approx 10^3$, the two contributions to the gauge field mass, $m^2_{2,\theta}$ and $\tilde{m}^2_B$ are comparable, as shown in figure 4.7, which does not hold for other values of ξ.

Both the particle number and the energy density can be computed equally well using the field $\theta_{\mathbf{k}}$ or $B^L_{\mathbf{k}}$, since the only moment for which the longitudinal gauge fields are not defined is when $\varphi(t) = 0$. At this instant we cannot define the particle number either way, since there is no well-defined adiabatic vacuum. Figure 4.8 shows the evolution of the particle number density for a few values of the comoving wavenumber after the first few inflaton zero-crossings, neglecting the effect of particle decays, as described in section 4.5. The left panel of figure 4.9 shows the particle number density per k-mode for $\xi = 10, 10^2, 10^3$ after the first inflaton zero-crossing. The condition of eq. (4.79) for the maximum excited wavenumber $k_{\rm max}$ is evident.

At this point, it is worth performing a simple estimate of the energy density that can be transferred to the gauge field modes away from the first point $\varphi(t) = 0$.

$$\rho = \int \frac{d^3k}{(2\pi)^3} n_k \omega_k \sim \langle n \rangle \, \tilde{m}_B \, k^3_{\rm max} \sim \langle n \rangle \left(\frac{10^5}{\sqrt{\xi}} H_{\rm end} \right) \left(\lambda^{3/2} m^3_{\rm pl} \right) \sim \langle n \rangle m^4_{\rm pl} 10^{-15} \xi^{5/2} \,, \tag{4.83}$$

where $\langle n \rangle$ is the average occupation number. The background inflaton energy density is $\rho_{\rm infl} = 3H^2 m^2_{\rm pl} \sim 10^{-11} m^4_{\rm pl}$, hence for $\xi \gtrsim 10^3$ the transfer of energy is enough to completely drain the inflaton condensate within one zero-crossing of $\varphi(t)$, if we take the particle number shown in figure 4.9 into account. The right panel of figure 4.9 shows the ratio of the energy density in gauge fields to the background energy density of the inflaton after the first zero-crossing. Obviously, values of $\rho_{\rm gauge}/\rho_{\rm infl} > 1$ are not physical but signal the possibility of complete preheating.

4.4.3 Unitarity scale cut-off

So far we have computed the excitation of gauge field modes of arbitrary wavenumber $k < m_{\rm pl}$. However the unitarity scale sets a limit above which no analytical (perturbative) treatment can be trusted. The unitarity scale for Higgs inflation and more generally for non-minimally coupled models, has received extensive attention in the literature. We will follow the analysis of Ref. [190], where a field-dependent unitarity scale was derived in both the Jordan and Einstein frames.

The unitarity scale at the end of inflation is $k_{\rm UV,1} \equiv m_{\rm pl}/\sqrt{\xi}$, which becomes $k_{\rm UV,2} \equiv m_{\rm pl}/\xi$ for even smaller values of the background Higgs field. It is straightforward to estimate the relation of the unitarity scale to the maximum excited wavenumber

$$\frac{k_{\rm UV,1}}{k_{\rm max}} = \frac{1}{\sqrt{\xi\lambda}} \sim \frac{5 \times 10^4}{\xi^{3/2}} \,, \tag{4.84}$$

$$\frac{k_{\rm UV,2}}{k_{\rm max}} = \frac{1}{\xi\sqrt{\lambda}} \sim \frac{5 \times 10^4}{\xi^2} \,. \tag{4.85}$$

We see that, depending on the value of the non-minimal coupling ξ, the wavenumber of the produced gauge bosons can exceed the field-dependent unitarity scale. New physics is needed above the unitarity scale and it is not clear how this new physics will change particle production for such large wavenumbers. We do not wish to propose any UV completion of the Standard Model in order to address the dynamics above the unitarity scale. We will instead provide a conservative estimate of the energy density in gauge bosons in the presence of unknown UV physics that suppresses particle production with large wavenumbers (above the unitarity scale). Simply put, we will compute the energy density by introducing a UV cut-off at $k_{\mathrm{UV},1}$ or $k_{\mathrm{UV},2}$.

If we consider the UV cut-off at $k_{\mathrm{UV},1}$, both $\xi = 10^3$ and $\xi = 10^4$ preheat entirely after one inflaton zero-crossing, since $k_{\mathrm{UV},1} \gtrsim k_{\mathrm{max}}(\xi = 1000)$, as can be seen from figure 4.9. If instead we place the UV cut-off at $k_{\mathrm{UV},2}$, the gauge fields do not carry enough energy to completely preheat the universe after one inflaton zero-crossing, regardless of the value of the non-minimal coupling ξ. We thus conclude that preheating into gauge fields is very sensitive to unknown UV physics, since the majority of the energy density is carried by high-k modes, whose number density in a UV-complete model can be much different than the one computed here. It is worth noting that the excitation of Higgs fluctuations occurs entirely below the unitarity scale, hence it is not UV sensitive. We will not consider any UV cut-off for the remainder of this chapter, unless explicitly stated.

4.5 Scattering, decay and backreaction

So far we have computed the parametric excitation of particles, either Higgs or gauge bosons, from the oscillating Higgs condensate during preheating. With the exception of the brief discussion in section 4.3.1, the interactions of the resulting particles have been completely ignored. However, as discussed in Refs. [171, 172], certain types of decays of the produced particles can suppress Bose enhancement and thus effectively shut off preheating. In Ref. [2] we carefully study the effects of the following decays and scattering processes:

A. the decay of Higgs particles into gauge bosons and fermions,

B. the scattering of Higgs particles into gauge bosons and fermions,

C. the decay of parametrically produced gauge bosons,

D. the scattering of gauge bosons into fermions and Higgs bosons and

E. possible effects arising from non-Abelian interactions of the produced W- and Z-bosons.

Any of the above mentioned processes can suppress or shut off the resonances. We summarize the results of Ref. [2] here.

4.5.1 Higgs decay

Decay of the Higgs into a pair of fermions f or gauge bosons B requires $m_h > 2m_{f,B}$. The fermion masses are

$$m_f^2 = \frac{y_f^2}{2}\frac{\varphi^2}{2f}\,, \tag{4.86}$$

while the gauge boson masses were extensively studied in section 4.4.2. Comparing the Higgs mass to the fermion and gauge boson masses shows that away from the zero-crossings of φ the only decay that is kinematically allowed is a decay into an electron-positron pair. The corresponding decay rate is given by

$$\Gamma = \frac{y_f^2}{8\pi} m_h\,. \tag{4.87}$$

For the electron, the small Yukawa coupling gives $\Gamma \ll H$, such that the decay is not efficient. We have checked that the instants where $\varphi \approx 0$ – and decay into other fermions is kinematically possible – are too short for significant Higgs decay to occur. We therefore conclude that perturbative decays do not shut off the self-resonance.

4.5.2 Higgs scattering

Due to the large number density, Higgs scatterings might be more efficient than decays. For Higgs scattering into pairs of bosons/fermions the kinematical constraint is weakened by a factor 2: $m_h > m_{f,B}$. As we saw above, kinematical constraints are significant, and we therefore only consider Higgs scattering into electron-positron pairs. The scattering rate is

$$\Gamma = n\sigma v\,, \tag{4.88}$$

where n is the Higgs number density, σ the interaction cross-section and v the velocity of the Higgs. We find that, despite the large number density, scattering is inefficient, $\Gamma \ll H$, due to the small cross-section $\sigma \propto y_e^4/(m_h^2)$. We also note that other scattering diagrams that could lead to Higgs depletion suffer from the same suppression factors as the tree-level scattering: light fermions have small Yukawa couplings, while heavy ones will lead to suppression factors from the fermion loops.

4.5.3 Gauge decay

Following Refs. [171, 172] the decay width of the W and Z bosons to fermions is given by

$$\Gamma_W = \frac{3g^2}{16\pi} m_W \,, \tag{4.89}$$

$$\Gamma_Z = \frac{g_2^2}{8\pi^2 \cos^2\theta_W} m_Z \left(\frac{7}{2} - \frac{11}{3}\sin^2\theta_W + \frac{49}{9}\sin^4\theta_W \right) , \tag{4.90}$$

where the decay widths are obtained by summing over all allowed decay channels into SM fermions. The decay of the Z boson to a pair of Higgs particles proceeds similarly. Using the gauge boson mass given in eq. (4.80), we see that $\Gamma_{W,Z}/H \gg 1$ and we find that decays into fermions completely deplete the produced gauge boson population within far less than a period of background oscillations. We estimate that the effect of particle decay *during* the Riemann spike is not strong enough to significantly affect the production of gauge bosons at the first zero-crossing. Hence, in order for the gauge bosons to be able to preheat the universe, the energy density in the gauge fields must be equal to the energy density in the inflaton condensate already after the first zero-crossing.

4.5.4 Gauge scattering

Instead of decaying into fermions, gauge bosons can also scatter into Higgs particles or fermion-antifermion pairs. The scattering rate is again given by $\Gamma = n\sigma v$, where v and n are now the velocity and number density of the gauge bosons respectively. We estimate

$$\frac{\Gamma}{H} \simeq \frac{10^5}{\xi^{3/2}} \,. \tag{4.91}$$

Since $\Gamma/H \lesssim 1$ for $\xi \gtrsim 10^3$, gauge field scatterings are not important for large values of ξ.

4.5.5 Non-Abelian effects

Since we are using an Abelian $U(1)$-gauge field as a proxy for preheating into SM W- and Z-bosons, we estimate the possible non-Abelian effects. As long as the linear analysis holds, the electroweak sector can be decomposed into 3 almost identical Abelian copies. However, once the the gauge field modes become sufficiently populated, their true non-Abelian nature cannot be neglected. Using a

Hartree-type approximation we can define the non-Abelian contribution to the gauge field mass-squared as $m^2_{\rm non-Abelian} \sim g^2\langle AA\rangle$. We estimate

$$\langle A^2\rangle \simeq 10^{-10}\xi m^2_{\rm pl}\,, \tag{4.92}$$

which does not dominate over the Riemann spike for $\xi \gtrsim 10^3$. We thus expect the explosive transfer of energy from the inflaton to the gauge fields for $\xi \gtrsim 10^3$ to persist even in the full $SU(2)_L \times U(1)_Y$ sector.

4.6 Observational consequences

As mentioned in section 2.1, observing reheating is difficult due to the inherently small length scales involved. However, there are two important quantities that can be used to connect reheating to particle physics processes or CMB observables: the reheat temperature $T_{\rm reh}$ and the number of e-folds of an early matter dominated epoch in the expansion history of the universe $N_{\rm matter}$.

4.6.1 Reheating temperature

The reheat temperature is computed using the Hubble scale at the instant when $\rho_{\rm infl} = \rho_{\rm rad}$ as

$$3m^2_{\rm pl}H^2 = \rho = \frac{\pi^2}{30g_*}T^4_{\rm reh}\,, \tag{4.93}$$

where $g_* = 106.75$ is the number of relativistic degrees of freedom at high energies. For instantaneous reheating from gauge field production, which happens for $\xi \gtrsim 1000$, the Hubble scale is $H \simeq H_{\rm end}$. For $\xi \lesssim 1000$ preheating proceeds through Higgs self-resonance, leading to a smaller value of the energy density as shown in figure 4.4. The monotonic increase of the reheat temperature $T_{\rm reh}$ as a function of the non-minimal coupling ξ is shown in figure 4.10. It must be noted that eq. (4.93) assumes the immediate transition to a thermal state after preheating has ended. For the case of Higgs self-resonance, this will occur through efficient scattering of Higgs bosons to the rest of the SM. For the case of instantaneous preheating to gauge fields, the situation is more complicated. In that case the number density of gauge bosons is not exponentially large, as is usually the case in preheating. On the contrary, the transfer of energy to gauge fields is done primarily through the production of fewer high-momentum modes $k_{\rm max} \sim \sqrt{\lambda}m_{\rm pl}$. A fraction of the produced W- and Z-bosons will decay to leptons, while another fraction will decay into quarks and antiquarks that

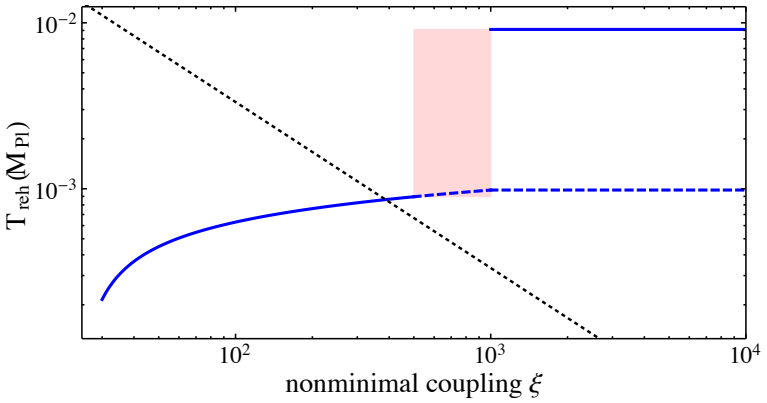

FIGURE 4.10: Reheat temperature in units of $m_{\rm pl}$ as a function of the non-minimal coupling ξ. The discontinuity at $\xi \simeq 10^3$ occurs due to the instantaneous preheating to gauge fields. The light red region represents the uncertainty of the exact threshold of instantaneous preheating to gauge fields. The black-dotted line corresponds to the unitarity scale constraint. The blue-dashed line shows the reheat temperature due entirely to Higgs self-resonance, assuming gauge boson production above the unitarity scale is suppressed due to unknown UV physics.

will eventually hadronize. The approach to thermal equilibrium will thus be more complicated. We leave the study of the thermalization process for future work and we use eq. (4.93) as an estimate of the reheat temperature, under the assumption of efficient thermalization.

However, a high reheat temperature may pose a challenge for any computation that goes beyond the linearized analysis that we presented, due to possible conflicts with the unitarity scale. Since thermalization of the reheating products will result in a blackbody spectrum, we can take the typical momentum involved to be $k \sim 3T_{\rm reh}$, which is thus the typical momentum exchange in particle scatterings inside the plasma. Since complete reheating means that the inflaton condensate will have completely decayed, the unitarity scale is $k_{\rm UV,2} \equiv m_{\rm pl}/\xi$. The typical particle momenta are below the unitarity scale for $3T < k_{\rm UV,2}$. As shown in figure 4.10, for $\xi \lesssim 300$, the resulting plasma has a low enough temperature to avoid processes that exceed the unitarity scale, at least neglecting the tail of the thermal spectrum. For $\xi \gtrsim 300$, the unitarity scale $k_{\rm UV,2}$ will be exceeded by the typical wavenumbers in the system, provided that thermalization is efficient. Finding out whether the unitarity scale is indeed violated for $\xi \gtrsim 300$ requires a more extensive study of the thermalization phase.

4.6.2 Number of matter-dominated e-folds

The duration of the reheating stage can have observational consequences, as was explained in section 2.1.2. The values of the spectral observables n_s and r are related to the time N_* when the CMB-relevant modes exited the horizon during inflation. For Higgs inflation and related models the CMB observables are given by $n_s \simeq 1 - 2/N_* - 3/N_*^2$ and $r \simeq 12/N_*^2$. Depending on the speed of the transition from the end of inflation to radiation-dominated expansion of the universe, the observationally relevant N_* may vary, shifting the predictions for n_s and r.

The number of matter-dominated e-folds of post-inflationary expansion is a non-monotonic function of the non-minimal coupling. For $\xi \gtrsim 10^3$, instantaneous reheating leads to a universe filled with gauge field modes of high wavenumbers, hence the universe transitions immediately to radiation domination (assuming no UV suppression). We must note that the decay of the inflaton condensate makes the gauge fields light, hence relativistic. For small values of the non-minimal coupling $\xi = \mathcal{O}(10)$, the background evolves as $w \approx 1/3$, hence the evolution of the universe is that of radiation domination soon after the end of inflaton, even if preheating is not efficient. Hence $N_{\rm matter} = 0$ for both large and $\mathcal{O}(10)$ values of the non-minimal coupling. There is an intermediate region of $\xi = \mathcal{O}(100)$, where preheating happens through self-resonance and the background evolves following an average equation of state of $w \approx 0$ [174] before preheating completes. In that regime of non-minimal couplings $N_{\rm matter} \approx N_{\rm reh} \approx 3$, slightly shifting the predictions of the CMB compared to the approximation of instantaneous reheating [119], where the equation of state is assumed to transition from $w = -1/3$ at the end of inflation to $w = 1/3$ immediately afterwards.

4.7 Conclusions

Higgs inflation is an appealing way to realize inflation within the particle content of the Standard Model, by coupling the Higgs field non-minimally to the gravity sector with a large value of the non-minimal coupling. We analyzed the non-perturbative decay of the Higgs condensate into Higgs bosons and electroweak gauge fields, finding distinct behavior for different ranges of values of the non-minimal coupling ξ.

The self-resonance of the Higgs field leads to preheating after $N_{\rm reh} \simeq 4$ e-folds for values of the non-minimal coupling $\xi \gtrsim 30$. For large values $\xi > 100$ the inflaton can transfer all of its energy into non-relativistic Higgs modes within $N_{\rm reh} \approx 3$, independently of the exact value of the non-minimal coupling. The dominant contribution to the parametric excitation of Higgs modes is the effect of

coupled metric fluctuations. In order to accurately capture the amplitude of the Higgs wavefunction, the computation must be initiated before the end of inflation.

The excitation of gauge bosons is much more dramatic, reminiscent of the purely scalar case of preheating in multi-field inflation with non-minimal couplings [174–176]. Gauge fields are excited after the first zero-crossing of the inflaton field, up to wavenumbers $k_{\rm max} \sim \sqrt{\lambda} m_{\rm pl}$. This leads to the possibility of the inflaton condensate transferring the entirety of its energy density to W- and Z-bosons immediately after the end of inflation, leading to instantaneous preheating. W- and Z-bosons will efficiently decay into SM fermions, ultimately filling the universe with a thermal plasma. Estimates of perturbative decay and non-Abelian effects show that gauge field production is robust against both for $\xi \gtrsim 10^3$.

The use of Coulomb, rather than unitary gauge for our computations allows us to tie the results to the purely scalar case studied in Refs. [174–176], as well as apply the results to other models with curved field-space manifolds. One such example is another version of Higgs and Higgs-like inflation, proposed in Ref. [210]. In that model, the necessary non-minimal coupling is small and negative, accompanied by a minimum of the Higgs potential at a large vacuum expectation value during inflation.

Another modification of Higgs inflation is based on the possible existence of an inflection point in the Higgs inflation potential [211–213]. The possibility of primordial black hole production in critical Higgs inflation has been proposed in Ref. [214]. It was however shown that large curvature fluctuations in Higgs inflation are hard or impossible to produce without violating observational limits on the tensor-to-scalar ratio and the running of the spectral tilt [215, 216], unless one postulates a large running of the non-minimal coupling ξ that is not found in the renormalization group flow of the Standard Model non-minimally coupled to gravity. Recent studies of Higgs inflation involving non-minimal couplings in the Palatini formulation of gravity [217, 218] can also have different preheating phenomenology. Exploring the preheating phenomenology of these models is interesting and can be performed using the techniques applied here. Such analyses can provide unique handles in order to probe the Higgs potential at energy scales that are out of reach for the LHC and any future accelerator.